RSC Advances

ROYAL SOCIETY OF CHEMISTRY

www.rsc.org/advances

Solar light driven Rhodamine B degradation over highly active β-SiC/TiO_2 nanocomposite

Gopa Mishra,[a, b] K. M. Parida,*[a, b] and S. K. Singh[a, c]

[a]Academy of Scientific and Innovative Research (AcSIR), Council of Scientific and Industrial Research, Anusandhan Bhawan, 2 Rafi Marg, New Delhi-110 001, India

[b]Colloids & Materials Chemistry Department, CSIR-Institute of Minerals and Materials Technology, Bhubaneswar, 751013, Odisha, India

[c]Advanced Materials Technology Department, CSIR-Institute of Minerals and Materials Technology, Bhubaneswar, 751013, Odisha, India

---

*Corresponding author

E-mail: paridakulamani@yahoo.com

Tel. no: +91-674-2581636-425

Fax: +91-674-25816

Abstract:

A series of β-SiC/TiO_2 nanocomposites were successfully fabricated by a sol-gel process with the purpose of efficient charge (e^-, h^+) separation and enhancement of photocatalytic performance under solar light irradiation. Pristine anatase state of TiO_2 was prepared by acid hydrolysis of Ti ($O^iPr)_4$ and β-SiC powder was synthesized by thermal plasma process from rice husk. The physicochemical characteristics of the nanocomposites were surveyed by X-ray diffraction (XRD), Fourier transform infrared spectroscopy (FTIR), UV-visible diffuse-reflectance spectroscopy (UV-Vis DRS), BET surface area, Transmission electron microscopy (TEM), X-ray photo electron spectroscopy (XPS), Field emission scanning electron microscopy (FE-SEM) and Photoelectrochemical (PEC) measurement. The PEC study confirms that TiO_2 is n-type semiconductor whereas β-SiC is p-type semiconductor. XRD, TEM and XPS study confirm the formation of hererojnction between β-SiC and TiO_2. The photocatalytic activities of all the β-SiC/TiO_2 nanocomposites were studied for aqueous Rhodamine B (Rh-B) dye degradation under solar light irradiation. The photo degradation mechanism of all the synthesized catalysts are further confirmed through chemical oxygen demand (COD) analysis and trapping of hydroxyl radicals by fluorescence probe technique. Among all the samples, 20 wt% β-SiC/TiO_2 exhibits a significant activity of 87% dye degradation in the presence of solar light. The high activity of 20 wt% β-SiC/TiO_2 is ascribed to high surface area, low crystallite size, high generation of OH radicals and COD efficiency.

Introduction

Over the past few decades, it has been reported that oxide based semiconductors are active photocatalyst in solar energy conversion for water decontamination and water splitting reaction.[1, 2] Among them, TiO_2 is one of the most promising semiconductor photocatalyst owing to its low cost, long-term stability, nontoxicity, high specific surface area and excellent photo catalytic property. However, there are two aspects which limits its application; (i) the wide band gap nature of TiO_2 (3.2 eV for the anatase phase or 3.0 eV for the rutile) makes it to absorb only ultraviolet (UV) light, (ii) to retard the recombination rate of photogenerated electron-hole pairs so that the excitons can be utilized effectively for organic pollutant degradation.[3] Therefore, efforts have been made to improve the photoabsorption of the UV active materials in the visible region and suppression of the recombination rate of the charge carriers.[4, 5] Moreover, in composite semiconductor materials, a heterojunction interface is constructed between the semiconductors with matching band potentials, and accordingly a contact electric field is built at the heterojunction interface. This electric field favors the transport of photogenerated charges from one semiconductor to another, leading to efficient separation of photogenerated electron-hole pairs and improves the efficiency of photocatalytic materials.[6] For photocatalytic application, the development of visible light responsive materials is necessary for proper utilization of solar light because it occupies 43% of the solar spectrum. Particularly, the coupling of n-type TiO_2 with p-type narrow band gap semiconductors is a good approach to improve the visible light absorption capability and photocatalytic performance of TiO_2 in presence of solar light.[7-10] In this context, several studies such as coupling of various semiconducting materials like Pt. TiO_2, Cu_2O/TiO_2, $TiO_2/N\text{-}Bi_2WO_6$, $CdS\text{-}TiO_2$ have been reported for Rh-B degradation under visible light irradiation.[10-13] But some of

these photocatalyst materials may not be easily recovered in pure form from the reaction mixture for further application. Some of the TiO_2 particle may be leached out into the solution even after centrifugation.

β-Silicon carbide (β-SiC) is an attractive narrow band gap (2.2 eV) p-type semiconductor prominently known for its interesting optical performance in the visible region and chemical stability during photocatalytic process.[14-17] The metal support stability (MSS) of SiC is higher and metal support interaction (MSI) is lower in comparison to any other catalytic materials.[14, 18, 19] Apart from the above features, cubic structured (3C-SiC) β-SiC exhibits excellent physical and chemical properties such as high thermal conductivity, low specific weight, insoluble in water and chemical inertness which are essential ingredients for heterogeneous catalytic reaction.[14, 20-22,] Up to now, a number of SiC/TiO_2 photocatalysts have been reported for photocatalytic performance under UV light.[20-22] It has been reported that the charge recombination rate is reduced in 3C-SiC/TiO_2 system used as photo electrode in dye-sensitized solar cell.[23] However, till today there has been no report on the degradation of Rh-B by sol-gel synthesized p-type β-SiC (derived from rice husk by plasma process)/n-type TiO_2 heterojunction based nanocomposite in presence of solar light. The heterojunction structure helps for visible light harvestation, easy channelization of photogenerated charge carriers which makes the system unique and pivotal for enhancing the photo catalytic efficiency in comparison to reported catalytic system.[10-13, 20-22]

In this present work, a series of β-SiC/TiO_2 nanocomposites with varying amount of β-SiC has been synthesized by sol-gel method and its characterization was carried out by various physiochemical techniques. The impact of β-SiC concentration on the crystal structure, morphology, optical properties of TiO_2 and photocatalytic

activity of β-SiC/TiO_2 nanocomposites towards Rhodamine B (Rh-B) dye degradation in the presence of solar light has been studied and discussed in details.

Experimental Section

Synthesis of β-SiC powder:

Rice husk was considered as a potential raw material for synthesis of silicon carbide.[24] Hence, in the present study the locally available rice husk was processed in plasma using indigenously developed 50 kW extended arc thermal plasma reactor with an applied load voltage of 50 V and an arc current of 300 A. The plasma forming argon gas flow was kept fixed at 1 L/min. The thermal plasma reactor provides very high temperature and rapid heat transfer which is the main advantage to convert rice husk to β-SiC within a short time period of 20 min. The detailed synthesis procedure was documented elsewhere.[25] The plasma synthesized product obtained from plasma reactor contained a mixture of β-SiC and a small percentage of carbon and silica. The plasma produced sample was heated at 700 °C in a Muffle furnace for 2 h to remove the free carbon. The particle size of the as synthesized β-SiC was found to be in the order of 10 μm. To further reduce the particle sizes, the plasma produced carbon free β-SiC powder was ground by Pulverisette 7 premium line planetary ball mill with 1.6 mm tungstate carbide (WC) balls. The grinding was carried out in 80 mL WC jar in isopropyl alcohol medium at a fixed rpm of 600 for 1 h. Then this ground sample was thoroughly washed with 1:1 HCl, 1:2 HNO_3 and 40% HF for the complete removal of silica and other metallic impurities (if any), present in the sample. The average particle size observed by Particle size analyzer (Model Nanotrac U2058I) was around 30-80 nm. This ground β-SiC nanopowder was taken as active material for the preparation of β-SiC/TiO_2 heterojunction based nanocomposites.

Synthesis of β-SiC/TiO_2 nanocomposites:

A series of β-SiC/TiO_2 heterojunction based nanocomposites were synthesized by a sol-gel process at room temperature by the hydrolysis of titanium (IV) isopropoxide (Ti (O^iPr)$_4$) in the presence of varying concentration of β-SiC powder, as illustrated in scheme 1. An requisite amount of β-SiC was dispersed in 30 mL of dry ethanol at room temperature followed by sonication for 30 min to break the agglomerated particles. Required amount of pure Ti (O^iPr)$_4$ was added drop wise to the suspension and stirred for other 30 min. Hydrolysis and condensation reactions of Ti (O^iPr)$_4$ was initiated through the addition of acetic acid (AA), followed by distilled water. The mixture was finally stirred in air at room temperature, resulting in a dry powder after total evaporation of the solvent. The dry powder was ground in a mortar to break the agglomeration. The resulting fine powder was calcined at 450 °C for 2 h in a conventional furnace to allow combustion of the remaining organic molecules and crystallization of the catalysts. In this way, different compositions of β-SiC (5, 10, 15, 20 and 25 wt% of β-SiC) loaded TiO_2 catalysts were prepared. Neat TiO_2 was prepared by acid hydrolysis of Ti (O^iPr)$_4$ in ethanol and calcined in a conventional furnace for 2 h at 450 °C. The nanocrystalline β-SiC & calcined TiO_2 were used as reference catalysts in this work.

Material characterization

The structure and phase identification of prepared samples were performed by X-ray powder diffraction (XRD) technique by Philips PANalytical PW 3040/60 instrument using Mo-Kα radiation of 0.7093 Å within 2θ range from 5 to 40˚. The bonding and structural information of all the prepared catalysts were recorded using Fourier transform infrared spectroscopy (FTIR) by Bruker-Alpha (ECO-ATR) within the range of 500-4000 cm^{-1}. Self supporting pellets were prepared with KBr and catalysts applying 50 kg/cm^2 pressure. These pellets were further used for recording

FTIR spectra. Optical absorbance of prepared catalysts were measured by UV-visible diffuse-reflectance spectroscopy (UV-Vis DRS), Varian Cary 100 spectrophotometer (model EL 96043181) equipped with a diffuse reflectance accessory in the region 200-800 nm. The spectra were recorded using boric acid as the reflectance standard. The BET surface areas of all the prepared samples were determined by N_2 adsorption-desorption studies at liquid nitrogen temperature (-197 °C) in an automated surface area and porosity analyzer (ASAP2020, Micromeritics, USA). The shape, size and composition of the prepared catalysts were determined by High resolution-transmission electron microscope (HR-TEM) equipped with energy dispersive X-ray (EDX) spectroscopy using TWIN FEI, TECNAIG^2 20 instrument operated at 200 kV. The electronic states of Ti, O, Si, C, has been examined by X-ray photoelectron spectroscopy ((XPS), Kratos Axis 165 with a dual-anode (Mg and Al) apparatus) using a Mg Kα source. All the binding energy values were calibrated by using the contaminant carbon (C1s=284.4 eV) as a reference. Charge neutralization of 2 eV was used to balance the charge of the sample. Binding energy values of the samples were reproducible within ±0.1 eV. The morphological and structural properties of the synthesized catalysts were studied by field emission-scanning electron microscopy (FE-SEM Zeiss Supra55) analyzer. The photoelectrochemical measurement (FE-SEM) was performed by potentiostat, (Versastat 3, Princeton Applied Research) using 300 W Xe lamps. For photoelectrochemical measurement, the electrodes were prepared by electrophoretic deposition in an acetone solution (30 mL) containing photocatalyst powder (30 mg) and iodine (30 mg). Two parallel FTO (fluorine doped tin oxide) electrodes were immersed in the solution with a 10-15 mm separation, and a 50 V bias was applied between the two for three min for potential control. The coated area was fixed at either 1 cm × 3 cm and then dried. The photoelectrochemical measurement

was performed using a conventional pyrex electrochemical cell consisting of a prepared electrode, a platinum wire as a counter electrode (1 mm in diameter, 15 mm in length), and Ag/AgCl reference electrode. The cell was filled with an aqueous solution of 0.1 M Na_2SO_4 and the pH of the solution was kept fixed to 6. The electrolyte was saturated with nitrogen prior to electrochemical measurements, and the potential of the electrode was controlled by a potentiostat (Versastat 3, Princeton Applied Research) with 300 W Xe lamps. Notably, the FTO did not show photo response in the solution. For $OH^{\bullet}$ radical detection the liquid PL (fluorescence spectrum) characterization was carried by LS-55 fluorescence spectrophotometer. The experiment was carried out in presence of solar light by taking 0.02 g L^{-1} of each catalyst with 5×10^{-4} M terephthalic acid (TPA) with a concentration of 2×10^{-3} M NaOH in 7 different tightly fitted conical flasks. The reaction solution of each individual catalyst was thoroughly centrifuged and taken by 5 ml of quartz cuvette with excitation wavelength of 315 nm.

Photocatalytic decolourisation process

The Rh-B dye (Fig. S1) degradation experiments in presence of solar light were carried out by taking 20 mL of Rh-B dye (100 mg L^{-1}), 0.02 g L^{-1} of each catalyst in 7 different tightly fitted conical flasks. The reactions were performed under 3 different conditions: (i) The control experiments were performed for 30 min under the dark condition in the presence of photocatalysts, to establish the adsorption of dyes on the active sites of the photocatalyst, (ii) degradation of the Rh-B was monitored under solar light for 3 h without using photocatalysts, (iii) finally, the degradation of the Rh-B was monitored in the presence of photocatalysts and solar light. The intensity of solar light was measured using a LT Lutron LX-101A digital light meter. The sensor was always set in the position of maximum intensity and the solar light intensity was

measured for every half an hour. The average light intensity was measured for the reaction, which was nearly constant during the experiment. Further the photocatalytic degradation activity of the β-SiC/TiO_2 composites and its comparison with the standard catalyst Degussa P25 was carried out in presence of visible light illumination ($\lambda \geq$ 400 nm) for 180 min in an irradiation chamber (BS 02, Dr. Grobel, UV-Elektronic GmbH). After irradiation, the dye suspensions were centrifuged and the remaining dye concentration was recorded using Carry 100 Varian UV-visible spectrophotometer (Model EL 96043181) at wavelength corresponding to the maximum absorbance of Rh-B (554 nm). The photocatalytic reactivity was estimated from the initial decrease in the concentration of dye after pre adsorption on the catalyst under dark condition.

For determining chemical oxygen demand (COD) of all synthesized materials during the photocatalytic processes, the aliquots were collected from each solution and taken for COD analysis by following a standard method reported in literature.[26] On the basis of the results, the photocatalytic degradation efficiency was calculated by the following equation (1)

$$\text{Photodegradation efficiency } (\eta) = \frac{\text{Initial COD} - \text{Final COD}}{\text{Initial COD}} \times 100 \qquad (1)$$

Results and discussion

XRD

Fig. 1 depicts the X-ray diffraction patterns of β-SiC/TiO_2 nanocomposites with varying amount β-SiC along with pure TiO_2 and β-SiC. The X-ray diffraction peaks in Fig. 1(a) indicates the presence of tetragonal anatase phase of TiO_2 with lattice planes (101), (004), (200), (105), (211), (204), (116), (220), (215) and (224) (JCPDS files No. # 21-1272). The X-ray diffraction peaks in Fig. 1(g) indicates the presence of neat cubic β-SiC phase with lattice planes (111), (200), (220), (311), (222) and (400)

(JCPDS files No. # 02-1050). The cubic β-SiC diffraction peaks begins to appear and gradually intensified upon increasing the β-SiC concentration over TiO_2 from 5-25 wt% (Fig. 1((b)-(f)). In addition, the intensity of the diffraction peaks of TiO_2 in β-SiC/TiO_2 nanocomposites become weaker. Further, the main diffraction peaks of TiO_2 in β-SiC/TiO_2 nanocomposites are slightly shifted to lower angle region compared to pure TiO_2, and the diffraction peaks of β-SiC are slightly shifted to a higher angle region in comparison to neat β-SiC sample. The maximum peak shifting has been observed in case of 20 wt% β-SiC/TiO_2 nanocomposites. The crystallite sizes of all the synthesized samples are determined by employing Scherer's formula ($D = n\lambda/\beta\cos\theta$), where λ is the wavelength of the X-ray (Mo-Kα), β is the full width at half-maximum of the diffraction peak, K is a shape factor (0.89) and θ is the angle of diffraction. The average crystallite size of TiO_2 and β-SiC are obtained as 12.27 nm and 12.49 nm respectively. However, in case of β-SiC/TiO_2 nanocomposite the crystallite size followed the trend: 20 wt% β-SiC/TiO_2 (10.39 nm) < 25 wt% β-SiC/TiO_2 (10.89 nm) < 15 wt% β-SiC/TiO_2 (11.07 nm) < 10 wt% β-SiC/TiO_2 (11.46 nm) < 5 wt% β-SiC/ TiO_2 (12.03 nm). The reason for the reduced crystallite size of SiC/TiO_2 nanocomposite is the result of close interaction between β-SiC and TiO_2 crystals in the heterojunction interface.[27, 28]

FTIR

FTIR patterns of β-SiC/TiO_2 nanocomposites together with pure TiO_2 and β-SiC are shown in Fig. 2. The more intense IR peaks at 835 cm^{-1} and 713 cm^{-1} attributes to the transverse optical mode of nano Si-C, bending vibration mode of Ti-O-Ti respectively.[29-31] The band at 3401 cm^{-1}, 1619 cm^{-1} and 2353 cm^{-1} attributes to stretching vibration mode of (-OH) hydroxyl group (free or bonded), bending vibration

of co-ordinated H_2O from the Ti-OH group, and stretching vibration mode of atmospheric CO_2, respectively.[32, 33] Apart from that, a small band arised at 954 cm^{-1} in β-SiC/TiO_2 nanocomposites attributes to the stretching mode of Si-O-Ti linkage.[30] It has been observed that after increasing the concentration of β-SiC over TiO_2 (Fig. 2(b)-(f)), the intensity of TiO_2 bands gradually decreases and shift towards the lower wave number region and at the same time, the peak width also increases. The maximum peak shifting at 20 wt% β-SiC/TiO_2 catalyst clearly confirms the strong interaction between β-SiC and TiO_2 in the heterojunction interface.

UV-Vis DRS

Fig. 3 shows the optical response of neat TiO_2, β-SiC and β-SiC/TiO_2 heterojunction based nanocomposites. The results point out that pure TiO_2 shows the absorption band at 387 nm (Fig. 3(a)) corresponding to UV light while the absorption band of β-SiC (Fig. 3(g)) lies at 566 nm corresponding to visible region. When TiO_2 combined with different concentration of β-SiC (5 to 25 wt%), the absorption band of all the combined samples has been extended gradually towards the visible region (Fig. 3(b)-(f)). This is due to the overlapping of the absorption band of the two components. The maximum visible light absorption in case of 20 wt% β-SiC/TiO_2 nanocompositeis only due to the contribution of narrow band gap β-SiC, since TiO_2 had no absorption in the visible region. This is also reflected in band gap calculation. The energy band gap of TiO_2, β-SiC and β-SiC/TiO_2 nanocomposite has been estimated from Taucs plot of $(\alpha h\nu)^{1/2}$ versus photon energy ($h\nu$).[34] The obtained band gap values has been summarized in Table 1. The calculated band gap energies of neat TiO_2 (3.2 eV) and raw β-SiC (2.19 eV) has been inserted in Fig. 3 as (a) and (g) respectively. The observed value are well consistent with that reported in litreture.[35, 14] The red shift of

absorption (towards 600 nm) in β-SiC/TiO_2 nanocomposite suggests the strong interaction between β-SiC and TiO_2 at the heterojunction interface, which make the catalyst active in solar light.[23]

BET Surface Area

In order to understand the textural properties, all the samples have been subjected to N_2 adsorption/desorption measurements. The results are summarized in Table 1. Surface area of TiO_2 is around 41.90 m^2g^{-1} with pore volume 0.1075 cm^3g^{-1}. With the increase of the β-SiC concentration, the surface area of all the β-SiC/TiO_2 nanocomposite increases. The increase in surface area may be due to the establishment of heterojunction and synergic effect between these two semiconductor.[28]

HR-TEM

Fig. 4 shows TEM images, selected area electron diffraction (SAED) pattern and energy dispersive X-ray (EDX) spectrum of β-SiC, TiO_2 and β-SiC/TiO_2 nanocomposites. It has been observed from TEM images that β-SiC particles are cubic in structure within the size range 30-80 nm (Fig. 4(a)) whereas TiO_2 nanoparticle are spherical in shape with an average diameter of 20-50 nm (Fig.4(b)). The respective SAED, EDX image shows that both β-SiC and TiO_2 particles are pure and polycrystalline in nature. The d values of 0.254 nm, 0.153 nm, 0.131 nm corresponding to cubic phase of β-SiC (JCPDS files No. # 02-1050) where the d values of 0.35 nm, 0.23 nm, 0.18 nm corresponding to tetragonal phase of TiO_2 (JCPDS files No. # 21-1272). From the EDX image (Fig. 4(c)-(g)), it has been clearly observed that intensity of Si and C peak gradually increases with respect to increase amount of SiC loading (5-25 wt%) over TiO_2 surface. The TEM image of Fig. 7(c)-(g), shows that β-SiC (5-25 wt%) particle are deposited on TiO_2 surface and the images are darker in

comparison to that of pure TiO_2 particles. Apart from that, a close contact between β-SiC and TiO_2 has been observed in the TEM morphology of 20 wt% β-SiC/TiO_2 sample (Fig. 7(f)) within the size range 20-100 nm. This type of morphology has been observed in case hetero junction, reported in litreture.[36, 37] Further, the SAED analysis support the co-existence of both β-SiC and TiO_2 phase in all β-SiC/TiO_2 nanocomposites. Fig. 5 describes the HR-TEM image of 20 wt% β-SiC/TiO_2 nanocomposite. From the micrograph, it has been clearly observed that well-defined lattice fringe separation with d = 0.35 nm of (101) plane corresponds to anatase phase of TiO_2 crystal where as the fringe separation with d = 0.25 nm of (111) planes corresponds to cubic phase of SiC crystals. The existence of intimate contact between β-SiC and TiO_2 indicates the formation of heterojunction between them. The formation of intimate junction is significant in the electron-transfer centre which leads the key role for higher photocatalytic activity. [36, 37]

XPS

Fig. 6 illustrates the XPS spectra of neat TiO_2, β-SiC and 20 wt% β-SiC/TiO_2 nanocomposites. The Ti 2p peaks of pure TiO_2 (Fig. 6(A)), shows the characteristic doublet at 458.93 eV (Ti $2p_{3/2}$) and 464.63 eV (Ti $2p_{1/2}$) with a peak separation of 5.7 eV, assigned to the Ti^{4+}state of TiO_2.[38, 39] The O 1s peak of pure TiO_2 with binding energy 530.6 eV in Fig. 6(B) assigned to bulk O^{2-} from TiO_2.[40, 41] The O 1s peak of β-SiC (Fig. 6(B)) at 532.3 eV, assigned to Si-O/hydroxyl group (OH) group, usually adsorbed on SiC surface.[42] The Si 2p peak of raw β-SiC in Fig. 6(C) shows a strong peak at 100.8 eV along with a small peak at 102.7 eV assigned to Si-C bond and Si-O bonds respectively.[42] The C 1s peak of pure SiC in Fig. 6(D) shows two peaks at 282.8 eV and 284.5 eV assigned to C-Si and C-C bonds in SiC lattice respectively.[42, 43] However, in 20 wt% β-SiC/TiO_2 nanocomposite the Ti 2p, the O 1s, Si 2p and C 1s

peak becomes wide and shift toward lower binding energy region from their original position (Fig. 6(A)-(D)). Apart from that, the peak arises at 102.42 eV (Fig. 6(C)) in case of 20 wt% β-SiC/TiO_2 composite, assigned to (Si-O-Ti) linkage.[44] This analysis is an indication of inter atomic interactions of TiO_2 with β-SiC/Si-O in the heterojunction of β-SiC/TiO_2 nanocomposites which results the peak shifting towards lower binding energy region. In case of heterojunction, such a shift in the binding energy has been observed in the literature.[45]

FE-SEM

Fig. 7 shows the morphology and elemental analysis (EDAX) of the neat TiO_2, β-SiC and β-SiC/TiO_2 nanocomposites with varying amount of β-SiC from 5 to 25 wt%. It has been observed that the β-SiC particles are semispherical, cubes and platelet like morphology within the size range from 30 to 100 nm. The EDAX graph (Fig. 7(a)) supports that the particles are composed of silicon and carbon. The TiO_2 particles are approximately uniform in size with spherical and hexagonal morphology (Fig. 7(b)). The EDAX graph (Fig. 7(b)) supports that the particle are composed of titanium and oxygen. The morphology of β-SiC/TiO_2 nanocomposite with variation of β-SiC concentration (from 5-25 wt%) are shown in Fig. 7(c)-(g). The EDAX graph (Fig. 7(c)-(g)) supports the presence of Si, C, Ti, and O element in β-SiC/TiO_2 composites. At 20 wt% β-SiC/TiO_2 nanocomposite, a close contact between TiO_2 particles and β-SiC grain edge has been observed which results a flower like morphology (Fig. 7(f)). In case of heterojunction, this type of morphology has been observed in the literature.[36, 37] The observed image of β-SiC/TiO_2 nanocomposite confirms the close interaction between SiC and TiO_2 at the heterojunction interface.

PEC Measurement

Fig. 8 displays the photocurrent spectra of β-SiC and TiO_2 at pH 6 *vs*. Ag/AgCl electrode. From the photocurrent spectra, it has been observed that TiO_2 generates an anodic photocurrent with applied bias suggesting as an n-type semiconductor. The flat band potential of TiO_2 has been observed at -0.95 V *vs*. Ag/AgCl at pH 6. The flat band potential is strongly related to the bottom of the conduction band and it has been considered as the conduction band minimum for n-type TiO_2.[46-48] Since the band gap energy of TiO_2 is 3.2 eV, the valence band maximum is estimated to be 2.25 eV. However, it has been observed that β-SiC generates cathodic photocurrent suggesting the p-type character of β-SiC. The photocurrent onset potential of β-SiC gives the value of the valence band edge maximum.[46-48] The photocurrent onset potential of β-SiC is observed at +0.84 V *vs*. Ag/AgCl electrode at pH 6, which has been considered as the valence band edge position of β-SiC.[46-48] The band gap energy of β-SiC is 2.19 eV. In consequence, the conduction band edge minimum is estimated to be -1.35 eV. The calculated band edge positions of p-type β-SiC and n-type TiO_2 has been represented in Scheme 2.

Photocatalytic activities

The percentage of Rh-B degradation over all the photocatalysts as a function of exposure time has been represented in Fig. 9. The percentage of dye adsorption follows the order: 25 wt% β-SiC/TiO_2 (14%) > 20 wt% β-SiC/TiO_2 (13.85%) >15 wt% β-SiC/TiO_2 (13%) > 10 wt% β-SiC/TiO_2 (11.1%) > 5 wt% β-SiC/TiO_2 (8%) > β-SiC (6%) > TiO_2 (5%) in corresponding with that of surface area. The percentage of Rh-B dye degradation over all the photocatalysts after 3 h of reaction under solar light follows the order: 20 wt% β-SiC/TiO_2 (87%) > 25 wt% β-SiC/TiO_2 (78%) > 15 wt% β-SiC/TiO_2 (72%) > 10 wt% β-SiC/TiO_2 (59%) > 5 wt% β-SiC/TiO_2 (52%) > β-SiC

(44%) > TiO_2 (33%). Fig. S2 shows a comparison of dye degradation (%) over β-SiC/TiO_2 composites along with Degussa P25 for 3 h of reaction under visible light. The percentage of Rh-B dye degradation under visible light follows the trend 20 wt% β-SiC/TiO_2 (82%) > 25 wt% β-SiC/TiO_2 (75%) > 15 wt% β-SiC/TiO_2 (70%) > 10 wt% β-SiC/TiO_2 (56%) > 5 wt% β-SiC/TiO_2 (50%) > β-SiC (44%) > TiO_2 (30%) > Degussa p25 (29%). From these experiments, it has been observed that the percentage of degradation increases with the increase of β-SiC concentration in the β-SiC/TiO_2 heterojunction nanocomposites up to 20 wt% and then decreases with further increasing the β-SiC concentration. Further the solar light is more effective for dye degradation over all the photocatalyst rather than visible light. Therefore, the decisive wt% ratio of β-SiC to TiO_2 has been found to be 20 wt% which exhibits the best photocatalytic activity towards Rh-B degradation over all the photocatalysts in presence of Solar light.

Chemical oxygen demand (COD)

The COD and COD efficiency of Rh-B dye solution after 3 h of solar light irradiation in all the prepared catalysts has been shown in Table 2. It has been observed that during the first hour of the experiment, the solutions are colored. The COD exhibits a substantial decolourisation of solution with time of irradiation. The reduction in COD values of the treated Rh-B solution indicates the suppression of electron-hole recombination and generation of more $OH^{\bullet}$ radicals in samples which plays an important role in the enhanced rate of photo mineralization of dye molecules. The percentage of COD efficiencies of Rh-B mineralization over all the photocatalysts follows the order: 20 wt% β-SiC/TiO_2 > 25 wt% β-SiC/TiO_2 > 15 wt% β-SiC/TiO_2 > 10 wt% β-SiC/TiO_2 > 5 wt% β-SiC/TiO_2 > β-SiC > TiO_2. The 20 wt%

β-SiC/TiO_2 nanocomposite exhibits noticeable faster decolourisation efficiencies of Rh-B over all the photocatalysts.

Kinetic Study

In addition, the kinetics of Rh-B degradation under solar light irradiation, over all the photocatalysts has been investigated by following Langmuir–Hinshelwood model.[49]

$$\ln (C_0/C) = kt$$

Here, k is the pseudo-first-order rate constant, C_0 is the initial concentration of the dye and C is the concentration of the dye in the reaction time 't' over all the photocatalysts. The apparent reaction rate constants (k) for the photocatalytic Rh-B degradation has been evaluated from experimental data using a linear regression. In all cases, the R^2 value is greater than 0.99, which confirms the proposed rate law for Rh-B degradation. The observed data follows pseudo 1st order kinetics for degradation process. The decreasing order of rate constants after 3 h of solar light irradiation has been summarized in Table 2 are as follows: 20 wt% β-SiC/TiO_2 > 25 wt% β-SiC/TiO_2 > 15 wt% β-SiC/TiO_2 > 10 wt% β-SiC/TiO_2 > 5 wt% β-SiC/TiO_2 > β-SiC > TiO_2, which corroborates the photocatalytic degradation results presented in Fig. 9. The corresponding k values of β-SiC/TiO_2 nanocomposites are much higher than that of pure β-SiC and TiO_2. Especially, 20 wt% β-SiC/TiO_2 nanocomposite exhibits the highest k value (0.011 min^{-1}) indicating that it has the best photocatalytic activity for decomposing Rh-B under solar light irradiation. The β-SiC/TiO_2 composites exhibit much higher photocatalytic activities than single phase β-SiC and TiO_2. The enhancement of the photocatalytic activities of the β-SiC/TiO_2 nanocomposites in comparison to individual components may be due to following two reasons: (i) the

formation of SiC/TiO_2 heterojunction as evidenced from HRTEM, XPS, XRD results. (ii) Further, it has been seen that β-SiC is capable of extending the absorption edge of TiO_2 to the visible region as explained in UV- Vis DRS spectrum. The heterojunction (p-n junction) formed between p-type β-SiC and n-type TiO_2 helps in separating the electron and hole pairs at the interface.

Mechanism of photodegradation

Fig. 10 describes the detailed mechanism of photo-excitation and simultaneous charge transfer process at the p-n junction interface of β-SiC/TiO_2 nanocomposite. The possible explanation for the quick and effective photodegradation of Rh-B over the β-SiC/TiO_2 nanocomposite has been explained with the help of following possible facts:

1. From the photo current spectra we found that β-SiC is a p-type semiconductor and TiO_2 is an n-type semiconductor. In favor of p-type β-SiC semiconductor, the Fermi level lies above the valence band whereas the Fermi level position below the conduction band for n-type TiO_2 semiconductor as shown in Scheme 2. As soon as p-type β-SiC combines with n-type TiO_2, a p-n junction is formed between them and the charge carriers diffuse in the opposite direction to form an electric field at the heterojunction interface. Under thermal equilibrium conditions, the Fermi level of n-type TiO_2 and p-type β-SiC are aligned in the middle position, and an internal electric field built to stop the charge diffusion between two semiconductors. In the meantime, the energy band positions of TiO_2 are shifted towards the downward direction and that of β-SiC towards upward direction along with Fermi level.[50, 28] This is known as a type-II band structure. According to the type-II band structure, conduction band (CB) and valence band (VB) of β-SiC lies above the conduction band (CB) and valence band (VB) of TiO_2. When solar light is supplied to the β-SiC/TiO_2 nanocomposite, β-SiC absorbs the photon of energy greater than the band gap energy, which excites the

electrons in the VB to the CB and leave the holes in the VB of β-SiC. The electrons in the conduction band of p-type β-SiC are then transferred to n-type TiO_2 and holes remain in the valence band of β-SiC. The migration of photogenerated charge carriers can be promoted by the inner electric field established at the heterojunction interfaces. Consequently, the photogenerated electron-hole pairs will be effectively separated due to the formation of junction between p-type β-SiC and n-type TiO_2 interface, resulting a reduced electron hole recombination.[50, 51] The separated electron and holes are then free to initiate the degradation reaction of Rh-B dye on the surface of photocatalyst.[51] The potential photocatalytic process in the degradation of Rh-B dye involves the following steps: (i) The CB electrons (e^-) accumulated on the surfaces of TiO_2 scavenged by oxygen molecule on the surface of the catalyst to form super oxide ($O_2^{-\bullet}$) radicals. These superoxide radicals again react with protons and photogenerated electrons to supply $HO_2^\bullet$ species which produce hydroxyl ($OH^\bullet$) radical in subsequent steps. (ii) Holes generated in the β-SiC surface may directly oxidize the organic species. The super oxide ($O_2^{-\bullet}$) radicals and hydroxyl ($OH^\bullet$) radicals are mostly responsible for the Rh-B dye degradation. The possible reaction mechanism for Rh-B dye degradation includes the following steps:

Catalyst (β-SiC/TiO_2) + hν → Catalyst (e_{CB-} + h_{VB+})

Catalyst (e_{CB-}) + O_2 → $O_2^{-\bullet}$

$O_2^{-\bullet}$ + H^+ → $HO_2^\bullet$

$HO_2^\bullet$ + $HO_2^\bullet$ → H_2O_2 + O_2

H_2O_2 → $2OH^\bullet$

Dye + $OH^\bullet$ → Dye product

Catalyst (h^+) + H_2O → Catalyst + H^+ + $OH^\bullet$

Dye + $OH^\bullet$ → Dye product

2. Fig. 11 explains the fluorescence emission spectrum of all the prepared photocatalysts after 3h irradiation. The intensity of the fluorescent peak at around 425 nm is directly proportional to the amount of $OH^{\bullet}$ radicals produced in water.[52] The greater the formation of $OH^{\bullet}$ radicals, higher the separation rate of e^- and h^+ pairs in the photocatalysts. Therefore, the photocatalytic activity has positive co-relation to the formation of radicals.[53, 54] The formation of hydroxyl radicals over all the prepared photocatalysts has been followed the order: 20 wt% β-SiC/TiO_2 > 25 wt% β-SiC/TiO_2 > 15 wt% β-SiC/TiO_2 > 10 wt% β-SiC/TiO_2 > 5 wt% β-SiC/TiO_2 > β-SiC > TiO_2, which agree well with photocatalytic activity.

Regeneration study and efficiency of the recycled materials

In order to regenerate the catalyst for further operation, 20 wt% β-SiC/TiO_2 after 3 h of reaction has been recovered by centrifugation, thoroughly washed with distilled water for several times and dried in an air oven. The dry powder has been used in the photocatalytic reaction with a fresh reaction mixture. Fig. S3 shows the recapability performance of the 20 wt% β-SiC/TiO_2 catalyst for 4 cycles. It has been found that the β-SiC/TiO_2 nanocomposite still retained a nearly same proportion of the original catalytic activity, even after 4 cycles. Thus, the 20 wt% β-SiC/TiO_2 catalyst had excellent operational stability.

Conclusions

β-SiC/TiO_2 nanocomposites can be successfully fabricated by a sol-gel process. The establishment of p-type β-SiC/n-type TiO_2 heterojunction has been confirmed by XRD, XPS and HRTEM results. The surface morphology, interaction between β-SiC and TiO_2 in β-SiC/TiO_2 nanocomposites are well explained by TEM, and FESEM study. The separation of the photogenerated charge carriers leads to enhanced

photocatalytic activities are supported by fluorescence spectra, photo-current measurement and COD analysis. The narrow band gap β-SiC extends the spectral response of TiO_2 from the UV to the visible region. Among all the catalysts, 20 wt% β-SiC/TiO_2 shows the highest result of 87% Rh-B dye degradation in the presence of solar light. The obtained p-type β-SiC/n-type TiO_2 heterojunction nanocomposite can be used as a potential solar light driven photocatalyst for further applications.

Acknowledgements

The authors are grateful to Prof. B. K. Mishra, Director, IMMT, Bhubaneswar, for his kind permission to publish this paper. The authors are acknowledged to Mr Ajit Dash, for his stable help in TEM analysis. The financial assistance by NWP-56 CSIR net working project is greatly acknowledged. The author Gopa Mishra is thankful to CSIR-New Delhi, for the award of SRF.

References

1 H. Zhang, G. Chen and D. W. Bahnemann, *J. Mater. Chem*., 2009, **19**, 5089-5121.

2 A. Kudo and Y. Miseki, *Chem. Soc. Rev.,* 2009, **38**, 253-278.

3 S. Martha, D. P. Das, N. Biswal and K. M. Parida, *J. Mater. Chem.,* 2012**, 22,** 10695-10703.

4 J. Bai, J. Li, Y. Liu, B. Zhou and W. Cai, *Appl. Catal. B,* 2010, **95**, 408-413.

5 Y. Xie, G. Ali, S. H. Yoo and S. O. Cho, *ACS Appl. Mater. Interfaces,* 2010, 2, 2910-2914.

6 J. Su, X. X. Zou, G. D. Li, X. Wei, C. Yan, Y. N. Wang, J. Zhao, L. J. Zhou and J. S. Chen, *J. Phys. Chem.C,* 2011, **115**, 8064-8071.

7 J. Yuan, H. Li, S. Gao, Y. Linb and H. Li, *Chem.Commun.,* 2010, **46**, 3119-3121.

8 N. Yildirim, T. Serin, and N. Serin, *J. Optoelectron. Adv. M.,* 2010, **12**, 1153-1156.

9 K. M. Parida and G. K. Pradhan, *Mater. Chem. Phys.,* 2010, **123**, 427-433

10 Y. Bessekhouad, D. Robert and J. V. Weber, *J. Photoch. Photobio. A,* 2004, **163**, 569-580.

11 E. A. Obuya, P. C. Joshi1, T. A. Gray, T. C. Keane, and W. E. Jones Jr, Int. J. Chem. 2014,6, 1-16.

12 M. Wang. L. Sun, Z. Lin, J. Cai, K. Xie, and C. Lin, ***Energy Environ. Sci.***, 2013, **6**, 1211-1220.

13 W. Li, X. Cui, P. Wang, Y. Shao, D. Li, F. Teng, *Mater. Res. Bull*., 2013, **48**, 3025–3031.

14 M. J. Ledoux and C. P. Huu, *Cattech.,* 2001, **5**, 226-246.

15 Q. B. Ma, B. Kaiser, J. Ziegler, D. Fertig, and W. Jaegermann, *J. Phys. D: Appl. Phys*., 2012, **45**, 1-6.

16 Y. Gao, Y. Wang and Y. Wang, *React. Kinet.Catal. Lett*., 2007, **91**, 13-19.

17 C. He, X.Wu, J. Shen and P. K. Chu, *Nano Lett.,* 2012, **12***,* 1545-1548.

18. R. Moene, L. F. Kramer, J. Schoonman, M. Makkee, and J. A. Moulijn, *Preparation of Catalysts VI Scientific Bases for the Preparation of Heterogeneous Catalysts,* 1995, Elsevier Science B.V, All right reserved. 371-380

19. R. Moene, E. P. A. M Tijsen, M. Makkee, and J. A Moulijn, *Appl. Catal. A-Gen.*, 1999, **184**, 127-141.

20. H. Yamashita, Y. Nishida, S. Yuana, K. Mori,M. Narisawa, Y. Matsumura, T. Ohmichi, I. Katayama, *Catal. Today*, 2007, **120**, 163-167

21 N. Keller, V. Keller, E. Barraud, F. Garin, and M. J. Ledoux, *J. Mater. Chem*., 2004, **14**, 1887-1895.

22 D. Hao, Zhenming Yang, Chunhai Jiang, Jinsong Zhang, *J. Mater. Sci. Technol*., 2013, 29, 11, 1074-1078.

23 Y. C. Lai and Y. C. Tsai, *Chem.commun.,* 2012, **48**, 6696-6698.

24 S. K. Singh, B. C. Mohanty and S. Basu, *Mater. Sci.,* 2002, **25**, 561-563.

25 S. K. Singh, L. Stachowicz, S. L. Girshick and E. Fender, *J. Mater. Sci. Lett.,* 1993, **12**, 459- 460.

26 ALPHA. *Standard methods for the examination of water and* wastewater, 20th ed.; American Public Health Association; Washington, DC, USA, **1998**.

27 X. Zhang, L. Zhang, T. Xie and D. Wang, *J. Phys. Chem. C,* 2009, **113**, 7371-7378.

28 J. Jing, X. Zhan, P. Sun and L. Zhang, *J. Phys. Chem. C,* 2011, **115**, 20555-20564.

29 J. Patyk, R. Rich, M. Wieligor and T. W. Zerd, *Acta. Phys. Pol. A,* 2010, **118**, 480-482.

30 A. Hilonga, J. K. Kim, P. B. Sarawade and H. T. Kim, *Powder Technol*., 2010, **199**, 284-288.

31 T. H. Suprabha, G. Roy, J. Thomas, K. P. Kumar and S. Methew, *Nanoscale. Res. Lett.,* 2009, **4**, 144-152.

32 Y. Gao, Y. Masuda, W. S. Seo, H. Ohta and K. Koumoto, *Ceram. Int.,* 2004, **30**, 1365-1368.

33 C. Matranga, L. Chen, M. Smith, E. Bittner, J. K. Johnson and B. Bockrath, *J. Phys. Chem. B,* 2003, **107**, 12930-12941.

34 J. Tauc, R. Grigorovici and A. Vancu, *Phys. Stat. Sol.,* 1966, **15**, 627-637.

35 G. Mishra, S. Mohapatra, S. Prusty, M. K. Sharma, R. Chatterjee, S. K. Singh, and D. K. Mishra, *J. Nanosci. Nanotechnol.,* 2011, **11**, 5049-5053.

36 J. Fu, B. Chang, Y. Tian, F. Xi and X. Dong, *J. Mater. Chem. A*, 2013, **1**, 3083-3090.

37 Y. Jia, S. Shen, D. Wang, X. Wang, J. Shi, F. Zhang, H. Han and C. Li, *J. Mater. Chem. A***,** 2013, **1**, 7905-7912.

38 B. Chai, T. Peng, X. Zhang, J. Mao, K. Li and X. Zhang, *Dalton Trans.,* 2013, **42**, 3402-3409.

39 D. Kumar, M. S. Chen and D.W. Goodman, *Thin Solid Films,* 2006, **515**, 1475-1479.

40 J. H. Richter, P. G. Karlsson, G. Westin, J. Blomquist, P. Uvdal, H. Siegbahn and A. Sandell, *J. Phys. Chem. C,* 2007, **111**, 3459-3466.

41 H. Park, H. G. Kim and W. Y. Choi, *Trans. Electr. Electron. Mater*., 2010, **11**, 112-115.

42 J. Binner and Y. Zhang, *J. Mater. Sci. Lett.,* 2001, **20**, 123-126.

43 G. Mishra, G. C. Behera, S. K. Singh and K. M. Parida, *Dalton Trans*., 2012, **41**, 14299-14308.

44 W. L. Yan, S. Y. Ping and X. B. She, *Chinese. Sci. Bull.,* 2008, **53**, 2964-2972.

45 D. Zhao, C. Chen, C. Yu, W. Ma and J. Zhao, *J. Phys. Chem. C,* 2009, **113**, 13160-13165.

46 D. W. Hwang, J. Kim, T. J. Parkand and J. S. Lee, *Catal. Lett.,* 2002, **80**, 53-57.

47 M. Long, W. Cai, and H. Kisch, *J. Phys. Chem. C* 2008, *112,* 548-554.

48 K. M. Parida, A. Nashim and S. K. Mahanta, *Dalton Trans.*, 2011, 40, 12839-12845.

49 J. Hou, Z. Wang, S. Jiao and H. Zhu, *Crystal Eng. Comm.,* 2012, **14**, 5923-5928.

50 J. Cao, B. Xu, H. Lin, B. Luo and S. Chen, *Dalton Trans.,* 2012, **41**, 11482-11490.

51 J. Zheng, Y. Zheng, C. Chen, Y. Zhan, X. Lin, Q. Zheng, K. Wei and J. Zhu, *Inorganic. Chem.,* 2009, **48**, 1829-1825.

52 K. M. Parida, L. Mohapatra and N. Baliarsingh, *J. Phys. Chem. C*, 2012, **116**, 22417-22424.

53 K. Ishibashi, A. Fujishima, Watanabe and T. K. Hashimoto, *Electrochem. Commun.,* 2000, **2**, 207-210.

54 H. Roussel, V. Briois, E. Elkaim, A. Roy and J. P. Besse, *J. Phys. Chem. B,* 2000, **104**, 5915-5923.

List of Schemes, Figures, and Tables with Captions

Scheme 1. Formation of β-SiC/TiO_2 heterojunction based nanocomposite photocatalyst by sol-gel technique.

Scheme 2. (a) The band edge position of p-type β-SiC and n-type TiO_2, calculated at pH 6 *vs* Ag/AgCl.

Fig. 1 X-ray diffraction patterns of (a) TiO_2, (b) 5 wt% β-SiC/TiO_2, (c) 10 wt% β-SiC/TiO_2, (d) 15 wt% β-SiC/TiO_2, (e) 20 wt% β-SiC/TiO_2, (f) 25 wt% β-SiC/TiO_2, and (g) β-SiC.

Fig. 2 Fourier transform infrared spectroscopy of (a) TiO_2, (b) 5 wt% β-SiC/TiO_2, (c) 10 wt% β-SiC/TiO_2, (d) 15 wt% β-SiC/TiO_2, (e) 20 wt% β-SiC/TiO_2, (f) 25 wt% β-SiC/TiO_2, and (g) β-SiC.

Fig. 3 UV-Vis Diffuse reflectance Spectroscopy of (a) TiO_2, (b) 5 wt% β-SiC/TiO_2, (c) 10 wt% β-SiC/TiO_2, (d) 15 wt% β-SiC/TiO_2, (e) 20 wt% β-SiC/TiO_2, (f) 25 wt% β-SiC/TiO_2 and (g) β-SiC.

Fig. 4 Transmission electron microscopy (TEM) Images, selected area electron diffraction (SAED) patterns and energy dispersive X-ray (EDX) spectrum of (a) β-SiC, (b) TiO_2, (c) 5 wt% β-SiC/TiO_2, (d) 10 wt% β-SiC/TiO_2, (e) 15 wt% β-SiC/TiO_2, (f) 20 wt% β-SiC/TiO_2 and (g) 25 wt% β-SiC/TiO_2 nanocomposite catalysts.

Fig. 5 A high-resolution transmission electron microscopy (HR-TEM) of 20 wt% β-SiC/TiO_2 nanocomposite catalyst.

Fig. 6 XPS spectrum of (A) Ti 2p, (B) O1s, (C) Si 2p, (D) C 1s for β-SiC, TiO_2 and 20 wt% β-SiC/TiO_2 nanocomposite catalysts.

Fig. 7 FESEM micrographs of (a) β-SiC, (b) TiO_2, (c) 5 wt% β-SiC/TiO_2, (d) 10 wt% β-SiC/TiO_2, (e) 15 wt% β-SiC/TiO_2, (f) 20 wt% β-SiC/TiO_2 and (g) 25 wt% β-SiC/TiO_2 nanocomposite catalysts.

Fig. 8 Current-Potential curves for (a) TiO_2, and (b) β-SiC under Xe light irradiation ($\lambda \geq 300$ nm).

Fig. 9 Photocatalytic activities of β-SiC, TiO_2 and different wt% of β-SiC/TiO_2 nanocomposites for Rh-B dye degradation under solar light.

Fig. 10 Mechanism of photo-excitation and simultaneous charge transfer process of p-type β-SiC/n-type TiO_2 nanocomposite for photocatalytic Rh-B dye degradation under solar light irradiation.

Fig. 11 Fluorescence emission spectrum of (a) TiO_2, (b) β-SiC, (c) 5 wt% β-SiC/TiO_2, (d) 10 wt% β-SiC/TiO_2, (e) 15 wt% β-SiC/TiO_2, (f) 20 wt% β-SiC/TiO_2 and (g) 25 wt% β-SiC/TiO_2 nanocomposite catalysts after 180 min irradiation.

Supporting information

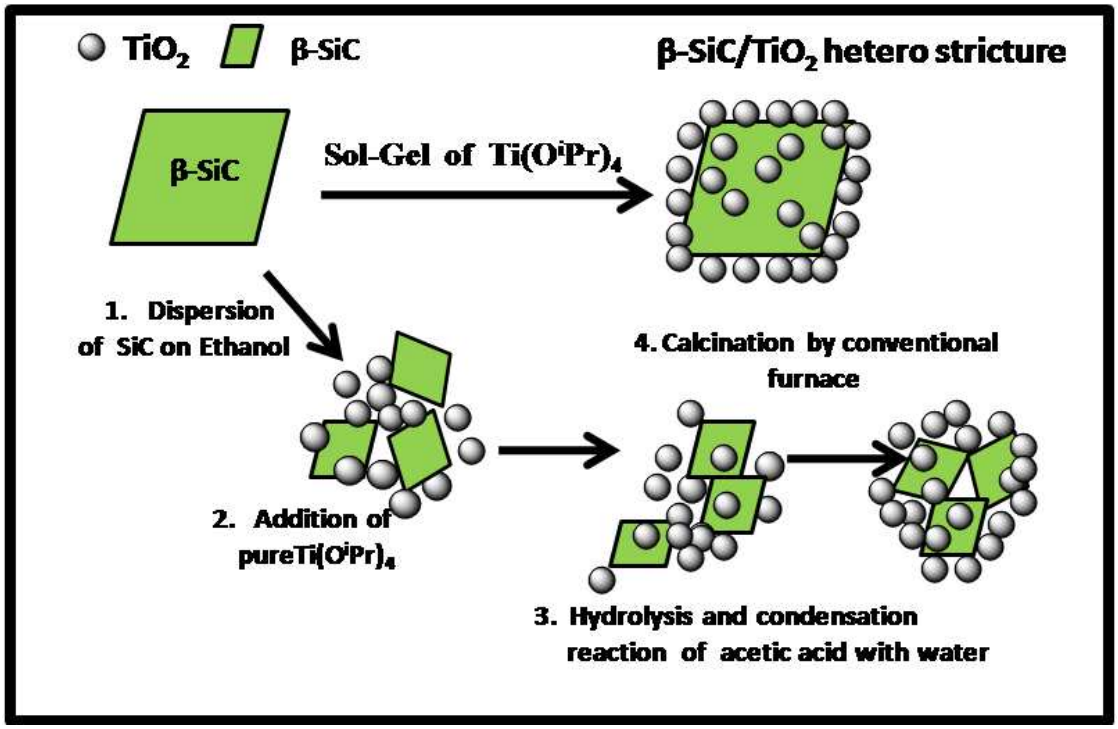

Scheme 1.

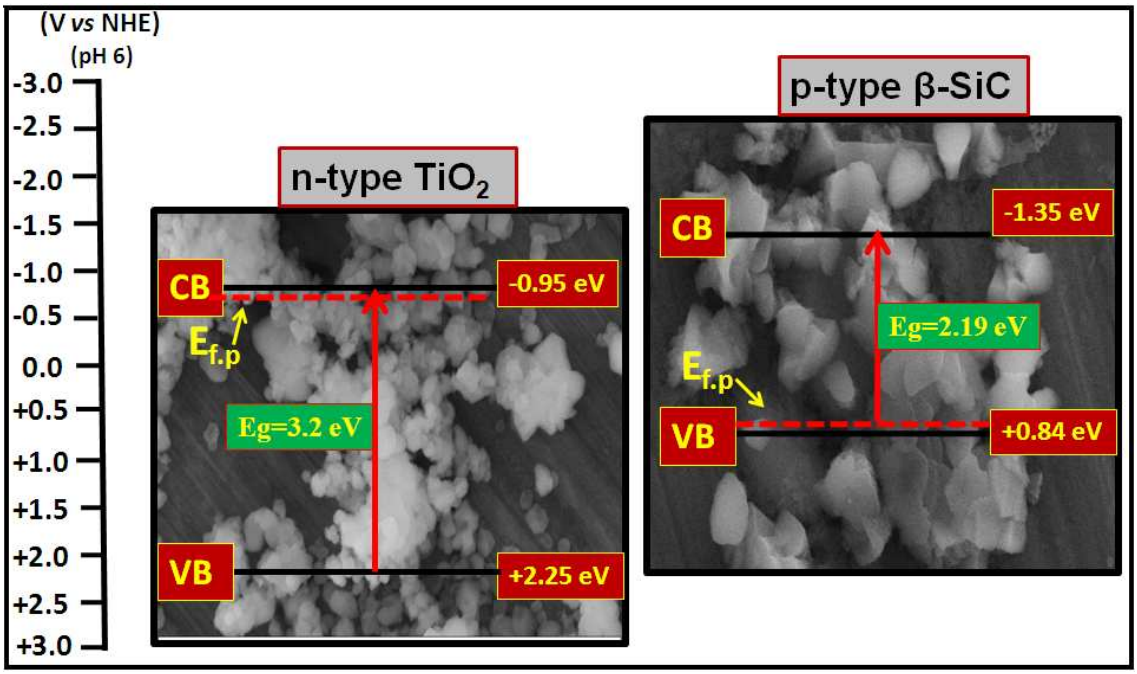

Scheme 2.

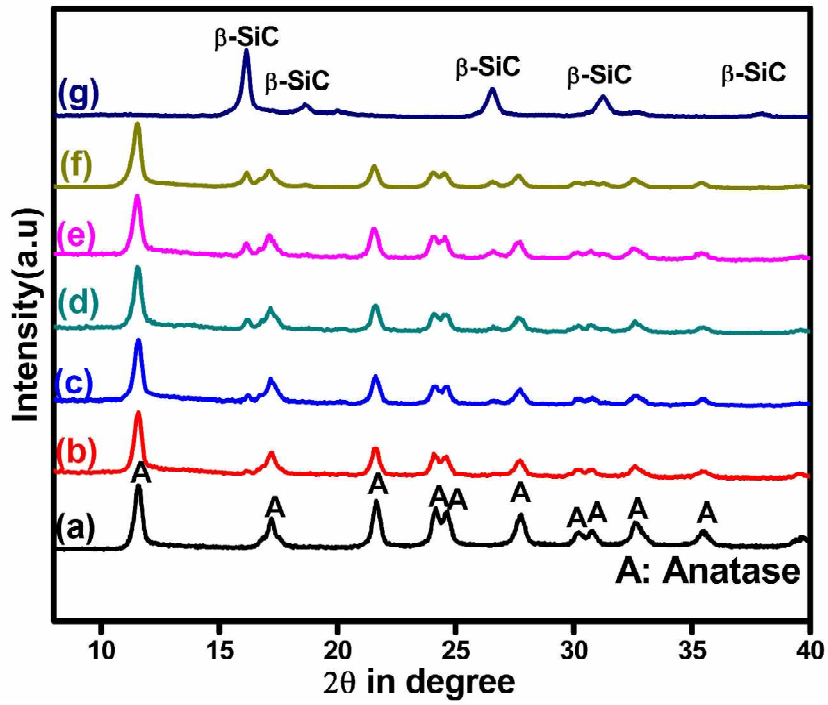

Fig. 1

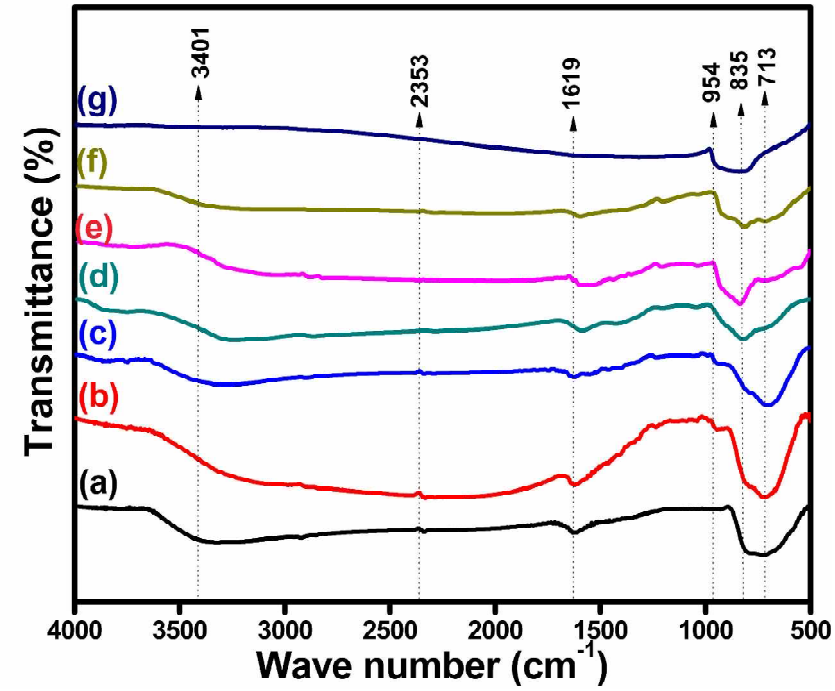

Fig. 2

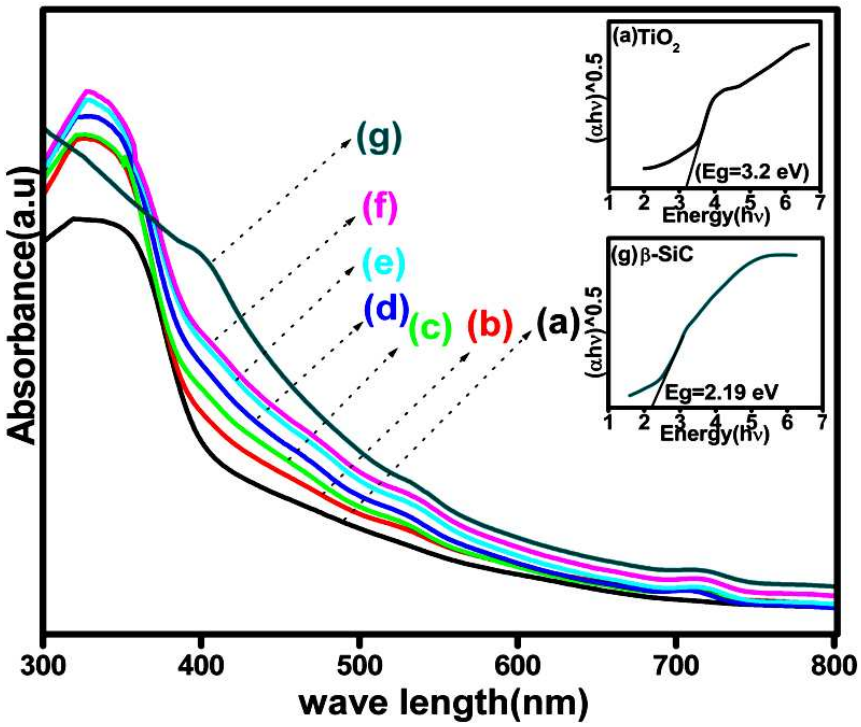

Fig. 3

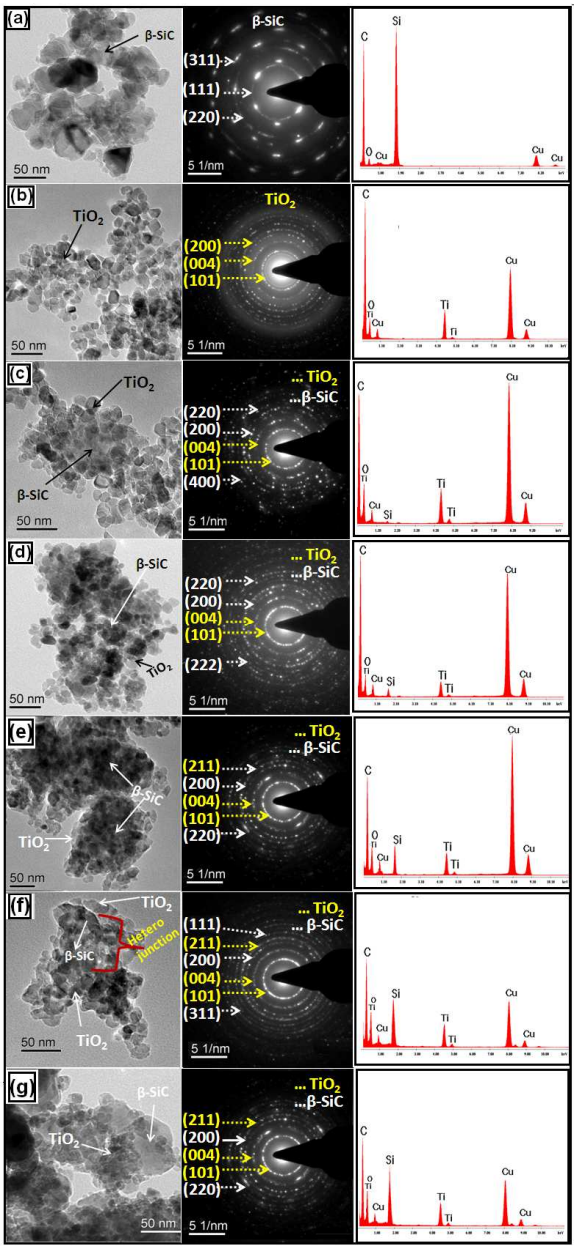

Fig. 4

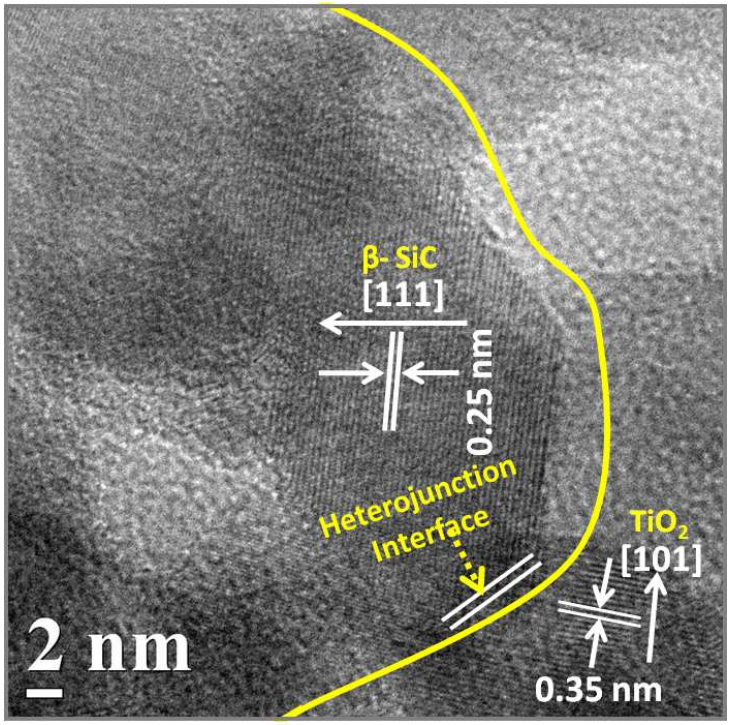

Fig. 5

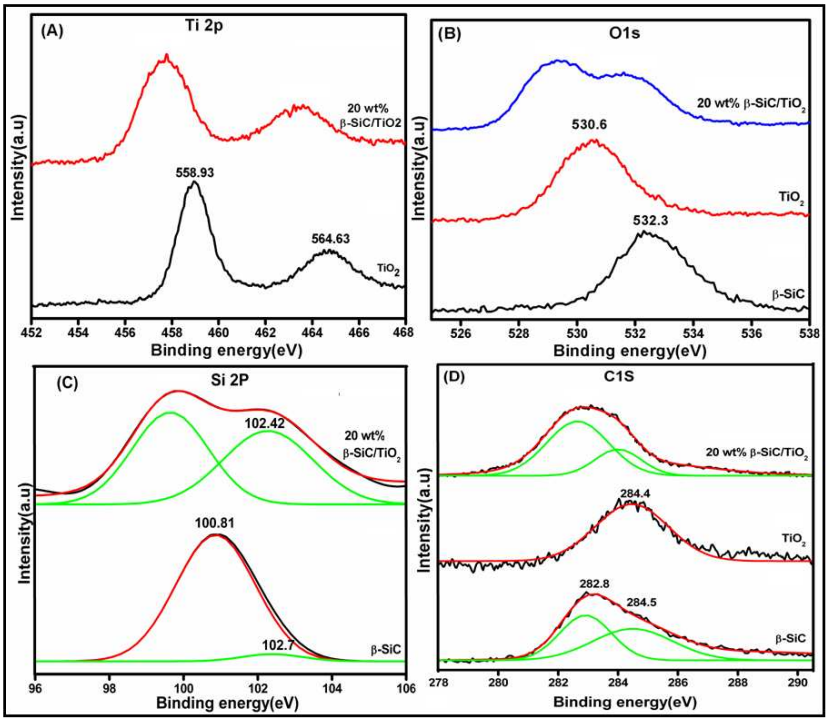

Fig. 6

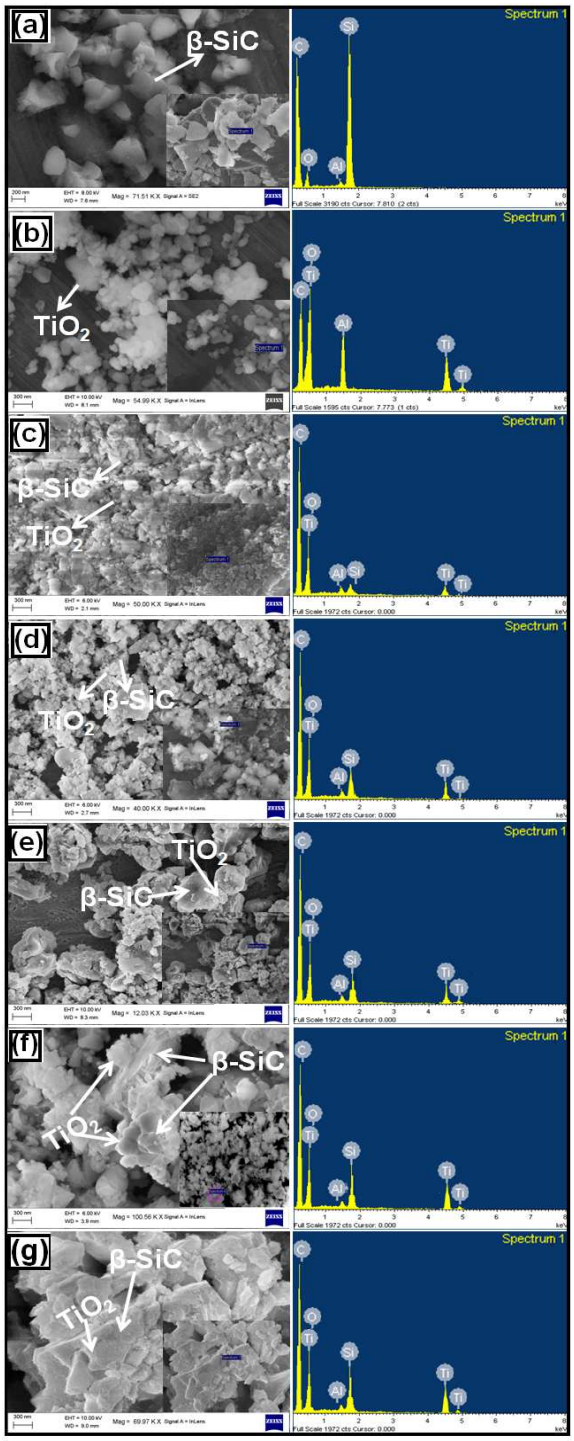

Fig. 7

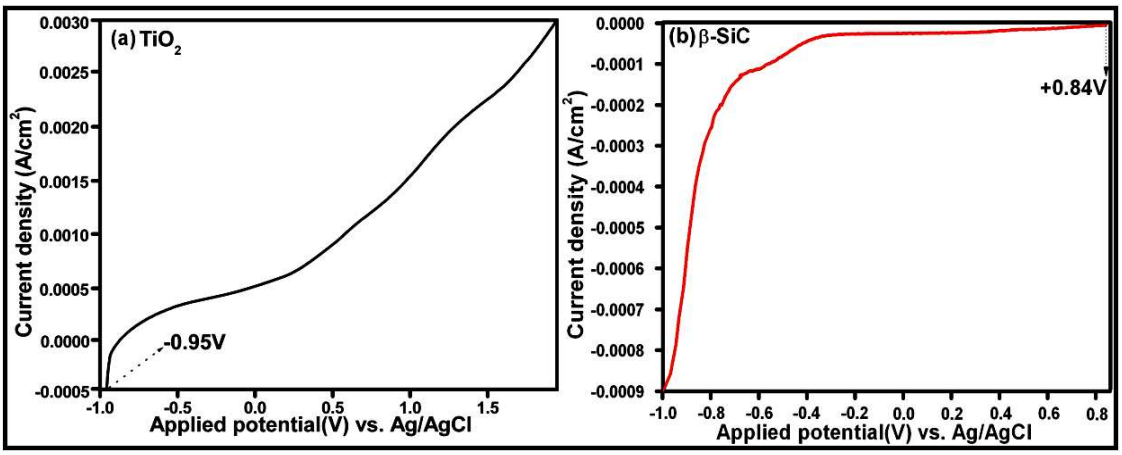

Fig. 8

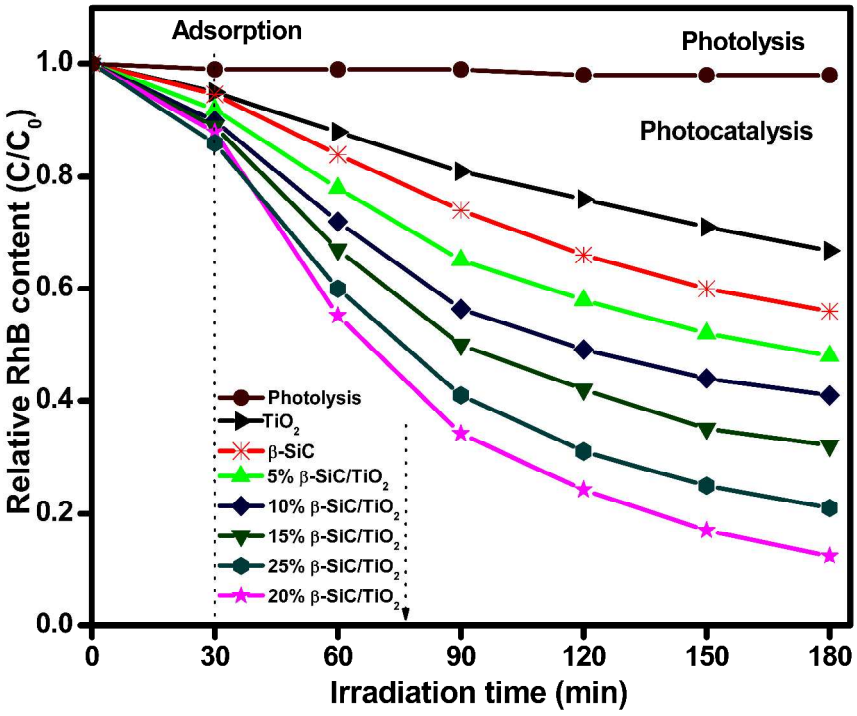

Fig. 9

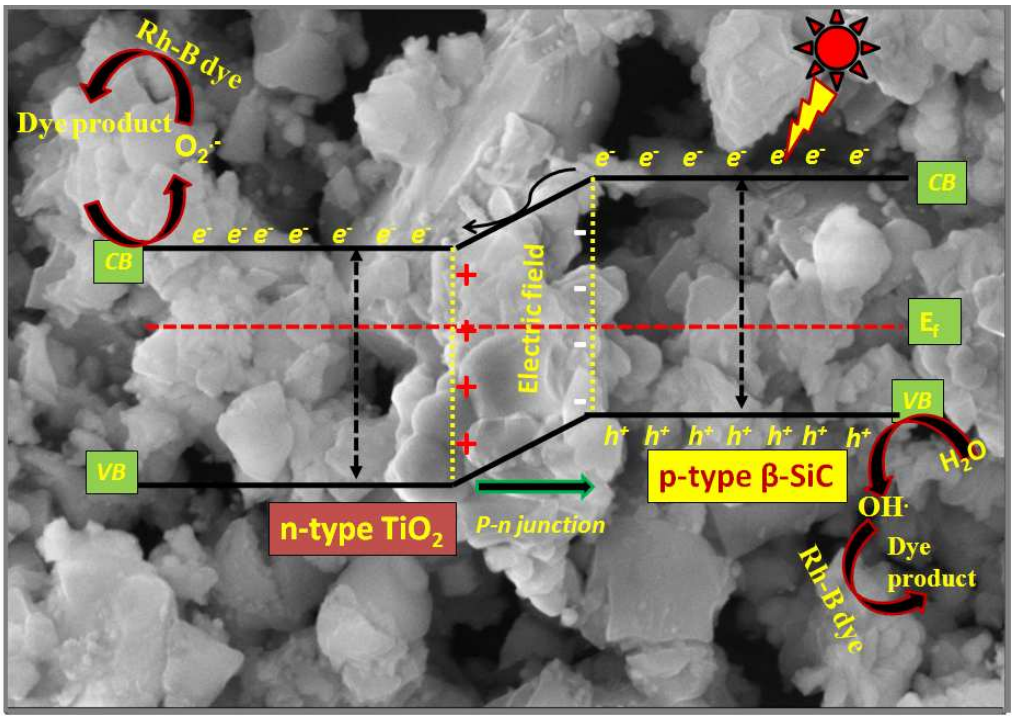

Fig. 10

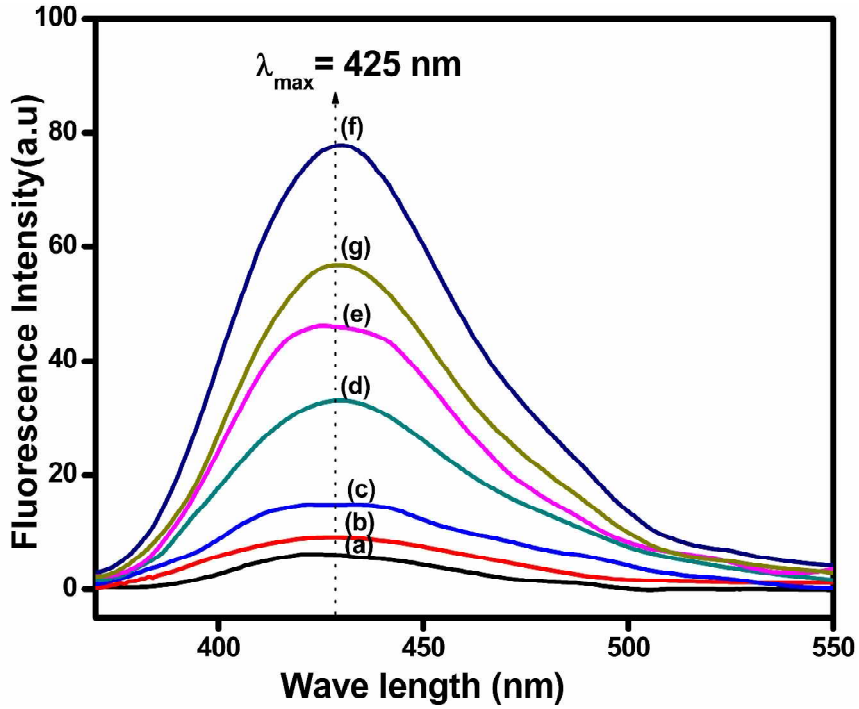

Fig. 11

Table 1. Textural and optical properties of the synthesized catalysts.

Catalyst	Surface area (m^2/g)	Pore size(nm)	Pore volume (cm^3/g)	Band gap energy(eV)
β-SiC	20	41.40	0.0462	2.19
TiO_2	41.90	17.87	0.2349	3.2
5 wt% β-SiC/TiO_2	44.48	13.44	0.1841	2.98
10 wt% β-SiC/TiO_2	56.18	11.47	0.1386	2.77
15 wt% β-SiC/TiO_2	72.49	11.09	0.1212	2.66
20 wt% β-SiC/TiO_2	85.12	10.66	0.1055	2.54
25 wt% β-SiC/TiO_2	83.27	11.3594	0.1127	2.50

Table 2. Pseudo-first order kinetics, COD (mg/L) and COD efficiency (%) of Rh-B dye over all synthesized catalysts.

Catalyst	k_{obs} (min^{-1})	R^2	COD (mg/L)	COD efficiency (%)
TiO_2	0.002	>0.9	58	31.129
β-SiC	0.004	>0.9	50.4	40.70
5 wt% β-SiC/TiO_2	0.006	>0.9	42	50.58
10 wt% β-SiC/TiO_2	0.007	>0.9	35.04	58.77
15 wt% β-SiC/TiO_2	0.008	>0.9	24.02	71.74
20 wt% β-SiC/TiO_2	0.011	>0.9	12.04	85.83
25 wt% β-SiC/TiO_2	0.010	>0.9	19	77.64

Graphics for Manuscript

Solar light driven Rhodamine B degradation over highly active β-SiC/TiO_2 nanocomposite

Gopa Mishra,[a, b] K. M. Parida,*[a, b] and S. K. Singh[a, c]

[a]Academy of Scientific and Innovative Research (AcSIR), Council of Scientific and Industrial Research, Anusandhan Bhawan, 2 Rafi Marg, New Delhi-110 001, India

[b]Colloids & Materials Chemistry Department, CSIR-Institute of Minerals and Materials Technology, Bhubaneswar, 751013, Odisha, India

[c]Advanced Materials Technology Department, CSIR-Institute of Minerals and Materials Technology, Bhubaneswar, 751013, Odisha, India

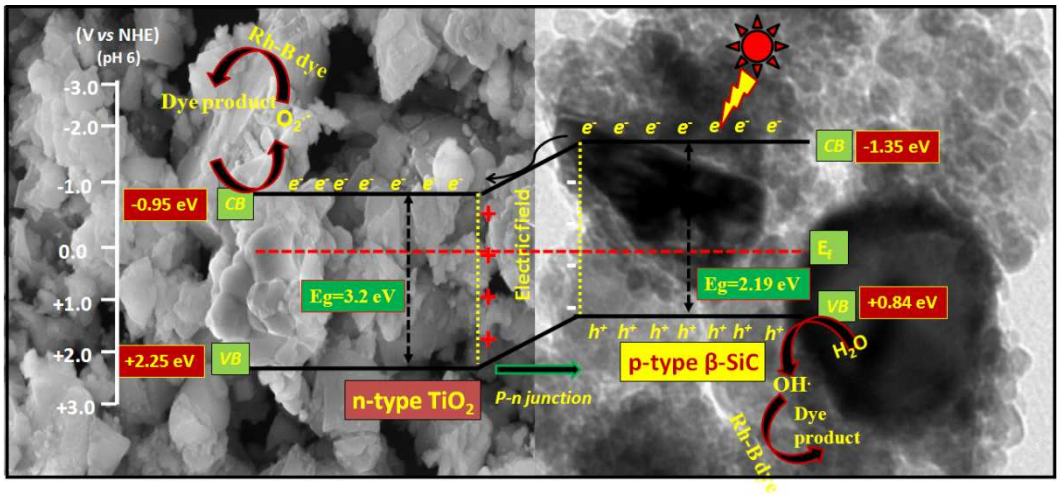

Heterojunction of β-SiC/TiO_2 nanocomposite photocatalyst has been synthesized by a facile technique. Catalyst is found to be robust enough to achieve high degree of Rhodamine-B degradation in presence of solar light.